J. Fluid Mech. (2009), *vol.* 633, *pp.* 1–16. © 2009 Cambridge University Press
doi:10.1017/S0022112009007666 Printed in the United Kingdom

Reactive Rayleigh–Taylor turbulence

M. CHERTKOV[1], V. LEBEDEV[1,2] AND N. VLADIMIROVA[1,3,4]†

[1]Theoretical Division and Center for Nonlinear Studies, Los Alamos National Laboratory, Los Alamos, NM 87545, USA

[2]Landau Institute for Theoretical Physics, Russian Academy of Sciences, Chernogolovka, Russia

[3]Department of Mathematics and Statistics, University of New Mexico, Albuquerque, NM 87131, USA

[4]ASC Flash Center, University of Chicago, 5640 S Ellis Avenue, Chicago, IL 60637, USA

(Received 24 July 2008 and in revised form 11 April 2009)

The Rayleigh–Taylor (RT) instability develops and leads to turbulence when a heavy fluid falls under the action of gravity through a light one. We consider a model in which the RT instability is accompanied by a reactive transformation between the fluids. We study the model using direct numerical simulations (DNSs), focusing on the effect of the reaction (flame) on the turbulent mixing. We discuss 'slow' reactions in which the characteristic reaction time exceeds the temporal scale of the RT instability, $\tau \gg t_{inst}$. In the early turbulent stage, $t_{inst} \lesssim t \lesssim \tau$, effects of the flame are distributed over a maturing mixing zone, whose development is weakly influenced by the reaction. At $t \gtrsim \tau$, the fully mixed zone transforms into a conglomerate of pure-fluid patches of sizes proportional to the mixing zone width. In this 'stirred flame' regime, temperature fluctuations are consumed by reactions in the regions separating the pure-fluid patches. This DNS-based qualitative description is followed by a phenomenology suggesting that thin turbulent flame is of a single-fractal character, and thus distribution of the temperature field is strongly intermittent.

1. Introduction

The Rayleigh–Taylor (RT) instability (Rayleigh 1883; Taylor 1950; Chandrasekhar 1961) occurs in many natural and man-made flows. Under constant acceleration, produced e.g. by gravity, the instability develops into the RT turbulence (Duff, Harlow & Hirt 1962; Sharp 1984), characterized by a mixing zone which continuously grows. Many recent experimental (Dalziel, Linden & Youngs 1999; Wilson & Andrews 2002), numerical (Dalziel *et al.* 1999; Cook & Dimotakis 2001; Young *et al.* 2001; Ristorcelli & Clark 2004; Cabot & Cook 2006; Vladimirova & Chertkov 2009) and theoretical efforts (Chertkov 2003; Chertkov, Kolokolov & Lebedev 2005) – last ones in the spirit of the turbulence phenomenology (Kolmogorov 1941; Obukhov 1949; Corrsin 1951; Frisch 1995) – have been devoted to analysis of turbulence inside the mixing zone. The mixing fluids can also be involved in chemical or nuclear reactions, e.g. flame. A flame front propagating against the acceleration is modified by the RT instability, which leads to a reactive turbulence in the mixing zone. Studies of the externally stirred turbulent flames belong to the general field of turbulent combustion (Damköler 1940; Williams 1985; Borghi 1988; Peters 2000; Kerstein 2002; Poinsot & Veynante 2005)

† Email address for correspondence: nata@flash.uchicago.edu

https://doi.org/10.1017/S0022112009007666 Published online by Cambridge University Press

and have many important applications. The buoyancy-driven, reactive turbulence is believed to be the dominant mechanism for thermonuclear burning in type Ia supernovae (Khokhlov 1995; Gamezo *et al.* 2003; Zingale *et al.* 2005). The interplay of buoyancy, reactive transformation and turbulence also plays a crucial role in studies of fusion (Freeman, Clauser & Thompson 1977) and large-scale combustion, such as furnaces and fires (Cetegen & Kasper 1996; Tieszen 2001). Turbulence, generated by buoyancy, facilitates mixing and thus counteracts the dynamical separation of fluids (phases) due to reaction. To explain this competition between separation and mixing is the main challenge emerging in the description of reactive flows (Kerstein 2002), which also applies in the broader context of multi-phase fluid mechanics, e.g. the RT turbulence of an immiscible mixture controlled by surface tension (Chertkov *et al.* 2005).

To clarify the nature of the competition between separation and mixing, let us consider a typical reactive RT setting. Initially, the heavy, cold reactant is placed on top of the light, hot product. As in the non-reacting RT instability, the mixing zone develops. Since locally the reaction occurs only in the mixed fluid, turbulence inside the mixing zone enhances the cumulative reaction rate. The effect of reaction, however, is the opposite – the reaction consumes mixed material and potentially limits the growth of the mixing zone. While diffusion and turbulence mix the reactant with the product, the reaction converts the mixed fluid into the product, thus causing an upward shift of the mixing zone as a whole.

In nature, this mechanism can take different forms. For instance, the flames in supernova are driven by conduction and fall into category of premixed combustion; reaction in liquids are driven by diffusion; and both mechanisms can be important for hydrocarbon combustion. In many cases the question of separation and mixing boils down to the question of energy transport and deposition. In numerical and theoretical studies, the reaction details are often omitted and replaced by reaction models. One-step reaction mechanisms are popular models, since they can represent both premixed and non-premixed reactions (Poinsot & Veynante 2005). These models describe the reactive transformation in terms of a single reaction progress variable. If the driving mechanism is the diffusion of heat, the reaction progress variable represents the temperature. If the driving mechanism is the diffusion of species, the reaction progress variable represents composition. When the Prandtl number (Pr) is equal to one, the reaction progress variable may represent either temperature or composition. Turbulence can enhance the reaction, in the first case by preheating the material (enhanced thermal diffusion) and in the second by enhancing the stoichiometry. One-step reaction models are used in whole-star supernova simulations (Khokhlov 1995) and are also frequently utilized in model studies of reactive RT instability (Vladimirova & Rosner 2005; Constantin, Lewicka & Ryzhik 2006).

Existing studies of reactive RT setting have mainly focused on the initial stages of instability (Lima, Van Saarloos & De Wit 2006) or on the instability restricted by container walls in experiments (Bockmann & Muller 2004) and by domain sizes in simulations (Khokhlov 1995; Vladimirova & Rosner 2005; Zingale *et al.* 2005). The transverse (to direction of gravity) confinement results in a constant (on average) cumulative reaction speed, presumably dependent on the domain size (Khokhlov 1995). In this system fluctuations, e.g. in velocity and density fields, do not grow with time. It is still not clear whether reaction can stabilize the unconfined RT instability. One suspects that the answer might depend on the relation between the time scale of the RT instability and the reaction time scale.

https://doi.org/10.1017/S0022112009007666 Published online by Cambridge University Press

In this paper we study RT turbulence unconfined by walls, in the presence of reactions slower than the RT instability. We consider the simplest (and still physically relevant) setting, the Boussinesq approximation, where the variations in the fluid density are small and are related linearly to the temperature contrast. The limit of small density variations is widely used in both experimental and numerical studies of the RT instability (Andrews & Spalding 1990; Linden, Redondo & Youngs 1994; Snider & Andrews 1996; Dalziel *et al.* 1999; Young *et al.* 2001; Ramaprabhu & Andrews 2004; Ristorcelli & Clark 2004). This limit is less common in traditional combustion applications, but it is often adopted in studies focusing on mixing and flame-turbulence interactions (Constantin *et al.* 2000; Peters 2000; Constantin, Kiselev & Ryzhik 2001; Kerstein 2002; Vladimirova *et al.* 2003). Autocatalytic reactions in liquids are often considered as models for premixed combustion and are sometimes referred to as 'liquid flames' (Lima *et al.* 2006).

Thus, our system can be modelled by the incompressible Navier–Stokes equation with the temperature-dependent buoyancy term, which is coupled with the advection–reaction–diffusion equation governing the temperature evolution. The set of equations is written as

$$\partial_t \boldsymbol{v} + (\boldsymbol{v}\nabla)\boldsymbol{v} = -\nabla p + \nu\nabla^2\boldsymbol{v} - 2\mathscr{A}\boldsymbol{g}\theta, \quad \nabla\boldsymbol{v} = 0, \tag{1.1}$$

$$\partial_t \theta + (\boldsymbol{v}\nabla)\theta = \tau^{-1}R(\theta) + \kappa\nabla^2\theta, \tag{1.2}$$

where $\boldsymbol{v}$ is the flow velocity; p is the pressure; and θ represents temperature variations and/or the chemical composition of the fluid. It is convenient to choose θ equal to zero in the cold (heavy) phase and unity in the hot (light) phase. Often, θ is referred to as the reaction progress variable. The reaction and production of heat is represented by the first term on the right-hand side of (1.2); we refer to $R(\theta)$ as the reaction rate function and to τ as the characteristic reaction time or reaction time scale. We consider a single-step reaction (see Poinsot & Veynante 2005), where the reaction rate is zero in the pure phases, i.e. $R(0) = R(1) = 0$ and $R = O(1)$ for $0 < \theta < 1$. The buoyancy force, i.e. the last term on the right-hand side of (1.1), is directed along the gravitational acceleration $\boldsymbol{g}$. The factor $\mathscr{A} = (\rho_1 - \rho_2)/(\rho_1 + \rho_2) \ll 1$ is the Atwood number, where ρ_1 and ρ_2 are densities of the reactant and the product, respectively. We assume that the kinematic viscosity ν in (1.1) and the diffusion coefficient κ in (1.2) are comparable, and thus the Prandtl number is of the order of unity.

The simplicity of the physical model allows us to analyse it using direct numerical simulations, that is resolving all hydrodynamical scales without subgrid modelling. Inspired by numerical simulations, we build a unifying phenomenological description explaining the interplay of turbulent mixing and reaction-mediated separation. Specifically, we focus on predicting macroscopic and microscopic features of the mixing zone, such as the upward transport of the mixing zone as a whole and statistics of density fluctuations within the mixing zone.

We compare our simulations with the benchmark non-reacting case, corresponding to $\tau = +\infty$ in (1.2). Phenomenological theory introduced by Chertkov (2003) and Chertkov *et al.* (2005) and hereafter called the 'phenomenology' suggests that in the non-reacting RT turbulence, velocity and density fluctuations are driven by buoyancy at the scales L_v and L_θ, respectively, both comparable to the mixing zone width H. These fluctuations generate cascades (of energy and temperature) towards small scales. The cascades terminate at the viscous scale η and (thermal) diffusive scale r_d, respectively (Chertkov 2003; Chertkov *et al.* 2005). The scales η and r_d are of the same order, provided the Prandtl number is of order unity. Previously conducted

https://doi.org/10.1017/S0022112009007666 Published online by Cambridge University Press

simulations of the non-reactive RT turbulence in the Boussinesq regime (Vladimirova & Chertkov 2009) show that while the mixing zone width grows in time, η and r_d decrease with time. It was also found that the correlation radii of both the velocity and temperature fluctuations L_v and L_θ grow in time as 0.05–$0.1H$. One special focus was on resolving the internal structure of the mixing zone more systematically than in the previous studies. It was shown that spatial correlations do not depend much on the vertical position within the mixing zone. In particular, this means that the relevant values of the major scales characterizing a snapshot of the RT turbulence depend only weakly on the height of the horizontal slice within the mixing zone.

2. Preliminary considerations

Our ultimate goal is to study the reactive RT instability in all regimes, from the non-reactive limit to the limit of fast reaction. In this paper we discuss the regime of relatively slow reaction: the time scale of the non-reacting RT instability t_{inst} and the characteristic reaction time τ are assumed to be well separated, $\tau \gg t_{inst}$. Here, t_{inst} can be estimated as the characteristic time of instability growth in the linear regime, $t_{inst} \sim \sqrt{Ag/\lambda}$, where λ is the typical size of the initial perturbation.

At the early stage, $t < \tau$, development of the mixing zone and the range of turbulent scales inside the mixing zone are weakly influenced by the reaction. Nevertheless a cumulative effect of the reaction can be seen in the overall shift of the mixing zone, as a whole, from the product side to the reactant side. To estimate the shift of the mixing zone z_f, let us integrate (1.2) along z. For the first term on the left-hand side one arrives at $\partial_t z_f$, while the only other non-zero contribution is associated with the reaction term R/τ on the right-hand side. Since in this regime the heat production is determined mainly by the mixing on the scale of the whole mixing layer, the reactive contribution is estimated simply as H/τ. Thus, $\partial_t z_f \sim H/\tau$. Even though the overall shift of the mixing zone at $t < \tau$ is smaller than H, z_f grows faster than H, so that the two scales become comparable at $t \sim \tau$. From this time onwards the reaction effects become more prominent.

The reaction becomes more effective when the turbulent turnover time at H, estimated as t, exceeds the characteristic reaction time τ. In this regime the reactant entrained into the mixing zone is burned out completely, and the overall shift of the mixing zone z_f should be of order H. This transition in the mixing zone evolution is also accompanied by a qualitative modification of the temperature fluctuations in the interior of the mixing zone. In contrast, the velocity distribution at all the scales is expected to show only weak sensitivity to the reaction even at $t > \tau$.

The two stages observed for $t < \tau$ and $t > \tau$ will be called the 'mixed stage' and the 'segregated stage', respectively. Although we deal with a continuously evolving state, at any given time we can consider a statistically quasi-steady pattern of mixing and separation inside the RT layer. It is interesting to put these patterns into the perspective of turbulent combustion, using the well-established classification of turbulent reactive systems. From this perspective (see Williams 1985; Peters 2000), the mixed regime is called a 'well-stirred reactor' (Poinsot & Veynante 2005), 'thickened flame (Borghi 1988) or 'broken reaction zone (Peters 2000), while the segregated regime is the regime of 'distributed reaction zones' (Poinsot & Veynante 2005), 'wrinkled–thickened flame (Borghi 1988) or 'thin reaction zone (Peters 2000). The transition between the regimes occurring at $t \approx \tau$ can be interpreted as crossing the $Da = 1$ line on the turbulent combustion diagram (see Poinsot & Veynante 2005). Indeed, the Damköler number Da (Damköler 1940) is defined as the ratio of the integral

https://doi.org/10.1017/S0022112009007666 Published online by Cambridge University Press

Run	τ	h_{lam}	s_{lam}
A	1600.00	160.00	0.10
B	177.78	53.33	0.30
C	64.00	32.00	0.50
D	40.32	25.40	0.63
E	16.00	16.00	1.00

TABLE 1. Laminar flame parameter for simulations discussed in the text: reaction time τ, laminar flame thickness $h_{lam} = 4\sqrt{\kappa\tau}$ and laminar flame speed $s_{lam} = 4\sqrt{\kappa/\tau}$ for KPP reaction.

time scale to the reaction time scale, $Da = t/\tau$, which grows linearly in time for the RT turbulence. The other popular dimensionless number in turbulent combustion, the turbulent Karlovitz number Ka describes the transition between the regime of distributed reaction zones/wrinkled–thickened flame/thin reaction zone and the 'flamelet' regime. The Karlovitz number is defined as the ratio of the chemical time scale to the Kolmogorov time scale. For the slowly reacting RT turbulence studied here, the flamelet regime does not apply; i.e. Ka is always much larger than unity, and it increases with time. The laminar flame regime is also not observed in the systems considered here; consequently the laminar flame thickness h_{lam} is an irrelevant scale.

At $t > \tau$ the main effect of the reaction on the mixing zone is in creation of domains of pure phases ($\theta = 0$ and $\theta = 1$). In these domains the fluctuations in the reaction term of (1.1) dominate fluctuations in the respective advection term, leading to complete suppression (burning out) of temperature fluctuations. The domains are separated by relatively thin (compared to domain size) interfaces at which burning occurs. The interface width, also referred to as the turbulent flame thickness L_f, (that is the scale at which the turnover time of velocity fluctuations is comparable to τ) becomes much smaller than L_v at $t \gg \tau$ due to the dominance of reaction.

Formation of the conglomerate of pure reactant and product domains should result in a qualitative transformation of the single-point statistics of the temperature field inside the mixing zone. A single-peak distribution centred around $\theta = 1/2$ transforms into a distribution with two peaks, related to the emergence of pure-phase domains corresponding to $\theta = 0$ and $\theta = 1$. The qualitative differences in the projected stages are summarized in figure 1 in which the temporal behaviour of different characteristics is shown schematically.

3. Numerical results

The computational technique used in this work is similar to that described in Vladimirova & Chertkov (2009). In our simulations, we use the popular Kolmogorov–Petrovskii–Piskunov (KPP) model (Fisher 1937; Kolmogorov, Petrovskii & Piskunov 1937), where $R = 4\theta(1-\theta)$ with $0 < \theta < 1$. The KPP model is not the only possible choice of the function $R(\theta)$. However, compared to other models, the KPP reaction provides a relatively thick laminar front which can be simulated at coarser resolution and makes computations more affordable. As before, we restrict ourself to the case of $Pr = 1$ and chose the units in which $\nu = \kappa = 1$ and $2\mathscr{A}g = 1$. The laminar flame parameters for five simulation sets discussed below are shown in table 1.

We solved (1.1) and (1.2) using the spectral element code developed by Tufo & Fischer (2001). We use elements of size 30^3 with 12 collocation points in each direction. The size of our computational domain is $960 \times 960 \times 1440$ physical units

https://doi.org/10.1017/S0022112009007666 Published online by Cambridge University Press

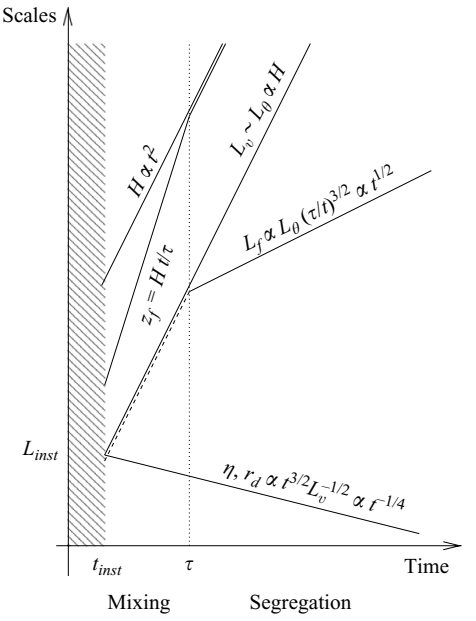


FIGURE 1. Schematic representation of the system evolution in log–log coordinates: the width of the RT mixing layer H, the large-scale fluctuations of velocity and temperature L_v and L_θ, the shift of the mixing layer z_f due to reaction, the turbulent flame thickness L_f and the dissipation scales η and r_d. The stages of the early RT instability development and transition to turbulence are shown shaded; τ is the characteristic reaction time, separating well-mixed and segregated regimes. In the mixed regime, the turbulent flame thickness corresponds to the typical width of interfaces, separating pure-phase domains of size L_θ. The temporal scalings are phenomenological propositions discussed in §§ 2 and 4.

or $384 \times 384 \times 576$ collocation points. We stop our simulation at time $t = 128$, when the width of the mixing layer approaches the size of the computational domain. The boundary conditions are periodic in the horizontal (x, y) directions and are characterized by no slip in the vertical (z) direction. The initial conditions, taken at $t = 0$, include a quiescent velocity and a slightly perturbed interface between the domains, determined by $\theta = \theta_0(z + \delta)$. The function $\theta_0(z) = 0.5[1 + \tanh(0.4z)]$ describes the density profile across the interface, and $\delta(x, y)$ is a perturbation having the spectrum with modes $18 \leqslant n \leqslant 48$ with spectral index 0. Here the spectral index refers to the exponent of the wavenumber (see Ramaprabhu, Dimonte & Andrews 2005), and it describes the shapes of the perturbation spectra.

The least processed results of numerical simulations, snapshots of the temperature field θ, are shown in figure 2; they are quite informative for our intuition. In run A ($\tau = 1600$) the structure of the mixing layer is practically indistinguishable from the non-reacting case (see Vladimirova & Chertkov 2009), at least up to $t = 128$. In run C ($\tau = 64$) the reaction starts to influence the temperature distribution somewhere between $t = 64$ and $t = 96$, where we observe emergence of regions of pure phases. In run E ($\tau = 16$) reactants and products are well separated by relatively thin interfaces at $t = 32$. Thus, a transition from the mixed stage to the segregated stage occurs at $t \approx \tau$, in accordance with the preliminary discussion of § 2.

In figure 2 we observe that the width of the mixing layer, defined as the vertical distance between bubbles and spikes, is approximately the same in all cases. Measurements of the half-width of the mixing layer, defined as $H = \int R(\bar{\theta})\,\mathrm{d}z$ (where

https://doi.org/10.1017/S0022112009007666 Published online by Cambridge University Press

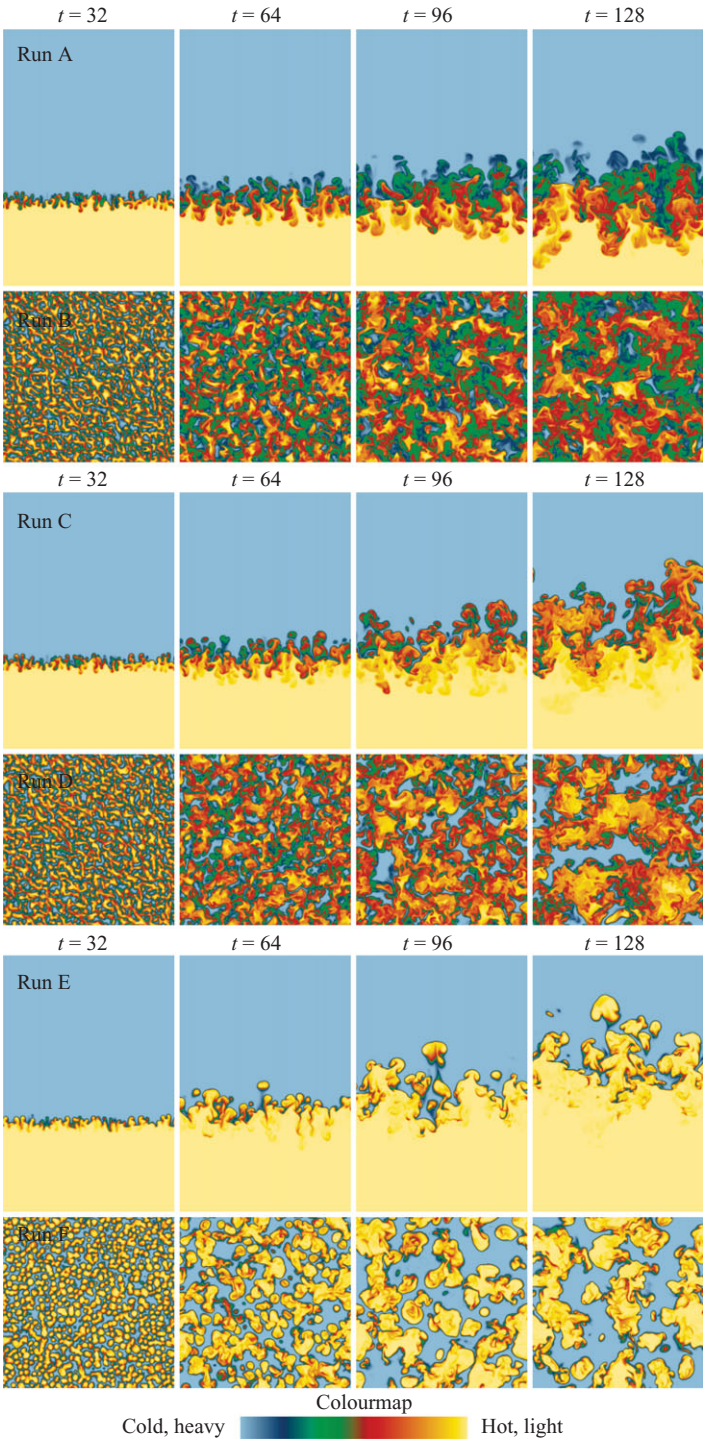


FIGURE 2. Vertical and horizontal ($z = z_f$, centre of the mixing zone) slices of temperature for three different reaction strengths.

https://doi.org/10.1017/S0022112009007666 Published online by Cambridge University Press

the overbar indicates averaging in a horizontal plane), confirm that $H(t)$ is weakly dependent on the reaction rate (see figure 3a). In figure 3(b) we plot the root mean square (r.m.s.) of the vertical velocity and see that in all five cases the r.m.s. velocity is practically the same. Moreover, all five cases exhibit similar internal structure of the velocity field inside the mixing layer, as we see from the comparison of the temperature and velocity correlation lengths L_θ and L_v measured in the central slice of the mixing zone (figure 3c). Following our earlier approach (Vladimirova & Chertkov 2009) we define the velocity correlation length L_v as the half-width of the the normalized two-point pair correlation function of velocity, $f(0)/f(L_v)=2$, with $f(r)=\langle v_z(\boldsymbol{r}_1)v_z(\boldsymbol{r}_1+\boldsymbol{r})\rangle/\langle v_z^2\rangle$. The temperature correlation function is defined in a similar way, but based on the temperature fluctuations, $\theta-\bar{\theta}$. Both temperature and velocity correlation lengths differ by 20–30 % compared to each other for τ ranging from 16 to 1600. Similar to what was reported in Vladimirova & Chertkov (2009) for the non-reacting case, $L_\theta/H\approx L_v/H\approx 0.1$. The viscous length $\eta=(\nu^2/\langle 5|\nabla v|^2\rangle)^{1/4}$ decreases slowly with time in all cases, with less than 10 % variation between $\tau=16$ and $\tau=1600$. The main conclusion here is that the velocity field is essentially insensitive to the reaction in the slow-reaction regime.

Next we look at the shift of the mixing layer $z_f=\int\bar{\theta}\,\mathrm{d}z$, introduced in § 2. We compute the cumulative reaction, or bulk burning rate, $\dot{z}_f=\int\overline{R(\theta)}\,\mathrm{d}z$, and compare it to the growth rate of the mixing layer $\dot{H}$. Both quantities are shown as functions of time in figure 3(d). We see that the bulk burning rate is greater for higher reaction rates. The time when $\dot{H}$ and $\dot{z}_f$ become comparable is approximately equal to τ.

It is not surprising that the bulk burning rate increases with decrease in τ. However, in addition to this obvious effect, we need to take into account the reaction efficiency, which depends on how well the fluids are mixed within the mixing layer. To quantify reaction efficiency, we use three related measures: $\dot{z}_f\tau/H$, the reaction rate averaged over the whole mixing layer; $\bar{R}(z_f)$, the reaction rate averaged over the middle slice; and Δ_{mix}, the fraction of well-mixed fluid in the middle slice, defined as a relative area of the slice occupied by fluid with $0.25<\theta<0.75$. In figure 3(e) we compare these quantities. Good agreement observed between the reaction rates averaged over the middle slice and the whole mixing layer suggests that the fraction of the well-mixed fluid within the mixing zone does not vary significantly with the vertical position. In fact, we had also made this observation earlier in our study of the non-reacting case (Vladimirova & Chertkov 2009), where the mixing efficiency $\overline{4\theta(1-\theta)}$ stayed at the constant level of ≈ 0.8 across the whole layer. We also see that Δ_{mix} behaves similar to $\bar{R}(z_f)$; some differences reflect an arbitrary choice of the selected limits. The area fraction Δ_{mix} as well as the average reaction rate in the middle slice and the reaction efficiency characterize the transition from the mixed stage to the separated stage. In the mixed stage Δ_{mix} is of order unity, and in the segregated stage it is a decreasing function of time. Numerical results, shown in figure 3(e), confirm a decrease of Δ_{mix} observed for $t>\tau$.

It is instructive to compare the states of the RT instability with different reaction rates at times corresponding to the same t/τ. Unfortunately, to get meaningful results, one must follow the evolution of the systems for times significantly exceeding the transition time. The same issue makes it difficult to measure the value of the α coefficient – the key parameter for the RT community, which is still under discussion even after decades of intensive work. Taking this difficulty into account we are pleasantly surprised that the plot of the burning efficiency versus t/τ demonstrates the alignment of the curves already within the limited time range available in our simulations (figure 4).

https://doi.org/10.1017/S0022112009007666 Published online by Cambridge University Press

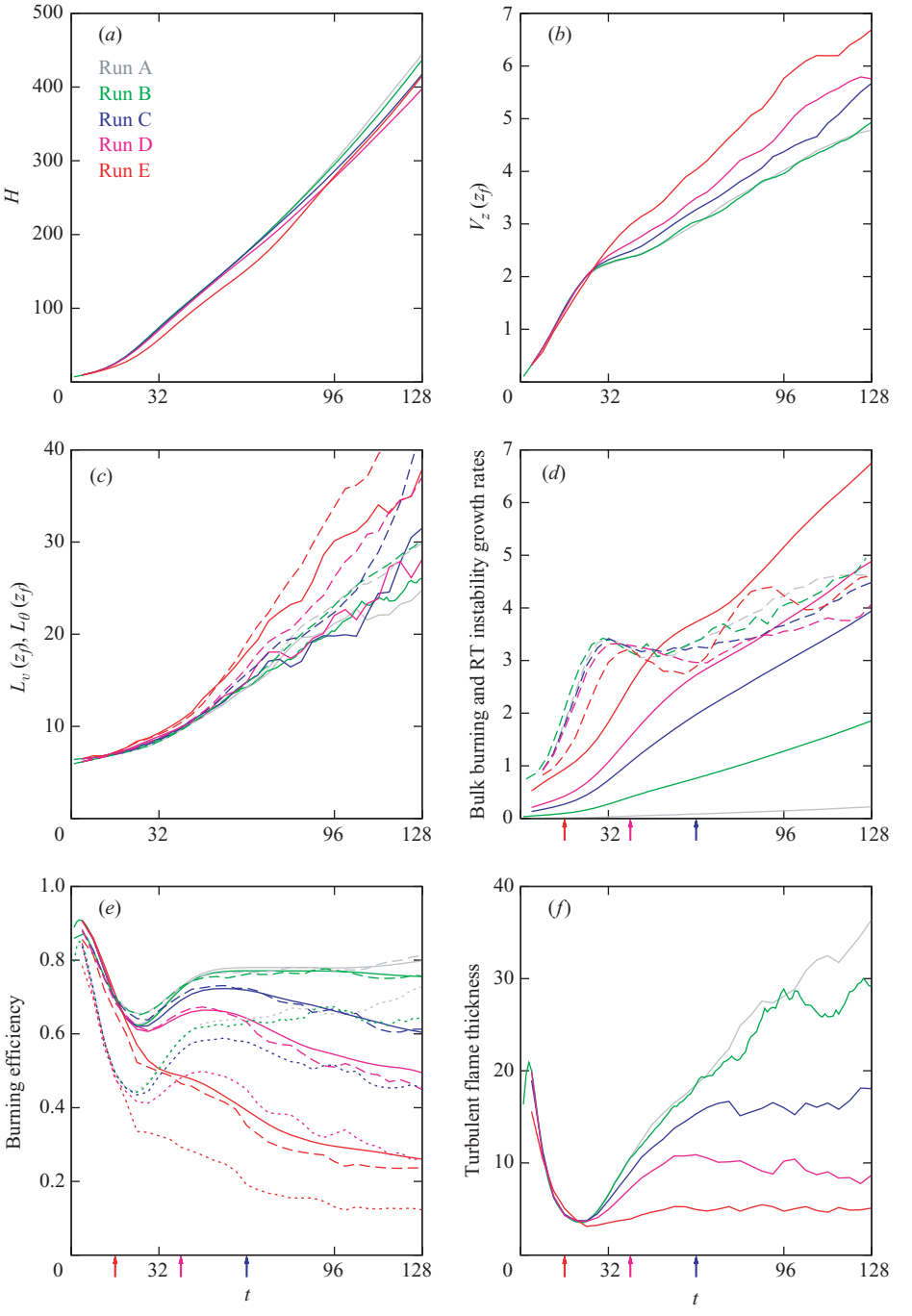


FIGURE 3. (*a*) Half-width of mixing layer H; (*b*) r.m.s. of vertical velocity at z_f; (*c*) pumping scale L_v (dashed lines) and scale L_θ (solid lines) measured at z_f; (*d*) bulk burning rate $\dot{z}_f$ (solid lines) compared to growth rate of RT instability $\dot{H}$ (dashed lines); (*e*) burning efficiency measured as ratio $\dot{z}_f\tau/H$ (solid lines), the average reaction rate $\bar{R}(z_f)$ in the middle slice (dashed lines) and well-mixed fraction of the slice area Δ_{mix} (dotted lines); (*f*) turbulent flame thickness in the middle slice obtained using 'expanding circle' technique. Arrows in (*d*) and (*f*) show the reaction time.

https://doi.org/10.1017/S0022112009007666 Published online by Cambridge University Press

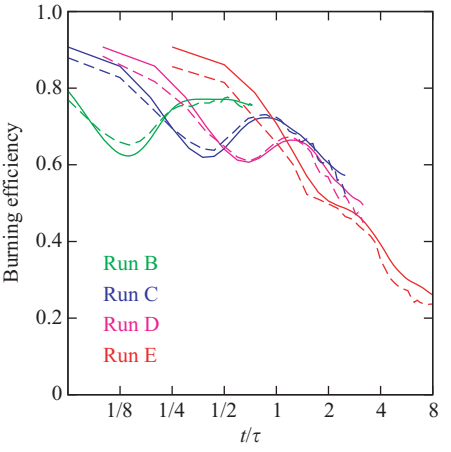


FIGURE 4. Burning efficiency measured as the ratio $\dot{z}_f \tau / H$ (solid lines) and the average reaction rate $\bar{R}(z_f)$ in the middle slice (dashed lines) as function of t/τ.

Since the reaction at the central slice ($z = z_f$) describes the bulk burning rate so well, we pay particular attention to the temperature distribution within the slice, shown in figure 5. In run A the probability distribution function (p.d.f.) of temperature evolves in time almost as if there were no reaction at all. It starts from a single-peak distribution determined by the initial conditions (slightly perturbed diffused interface). Then, during the linear stage of the RT instability, $t \lesssim 16$, the p.d.f. transforms into the two-peak shape and becomes single peaked again at $t \approx 48$. The transformation from one to two peaks corresponds to the transition to the nonlinear regime of the RT instability, associated with secondary Kelvin–Helmholtz-type shear instability and formation of RT mushrooms, while transition from two peaks to one corresponds to the destruction of RT mushrooms and formation of the turbulent mixed zone. When reaction is stronger, as in runs B and C, we observe yet another transformation in the p.d.f., namely the appearance of a narrow peak around $\theta = 0$ and decrease in the middle of the θ range at $t \approx \tau$. The transition to the two-peaked shape at $t \approx \tau$ is of interest to us, since it indicates transition to the segregated regime. (In runs D and E, this one-two-one-two peak pattern is not noticeable because τ is of the order of, or shorter than, the transition time from linear RT instability to nonlinear RT instability.) Quantitatively the process of the transition to the segregated regime can be described by integrating the p.d.f. over some interval in the vicinity of $\theta = 1/2$. Selecting the interval $0.25 < \theta < 0.75$, we obtain Δ_{mix}, described earlier.

The well-mixed fraction Δ_{mix} is related to the turbulent flame width L_f or the width of the layer separating the pure-phase domains. Aiming to study the geometry of the turbulent flame we measure L_f in the following way: for each point with $1/4 < \theta < 3/4$ we find the largest radius of the circle around this point containing only points with $1/4 < \theta < 3/4$; this length, averaged and multiplied by four, represents the typical width of the burning region L_f, shown in figure 3*f*. We observe that (i) L_f increases with τ; (ii) $L_f \sim L_\theta$ for $t < \tau$ (compare figure 3*f*′), and L_f grows with time but slower than L_v, and so L_f / L_v decreases with time.

To summarize, we have observed in our numerics the transition at $t \approx \tau$ from mixed regime to segregated regimes in variety of ways, from visual comparison of

https://doi.org/10.1017/S0022112009007666 Published online by Cambridge University Press

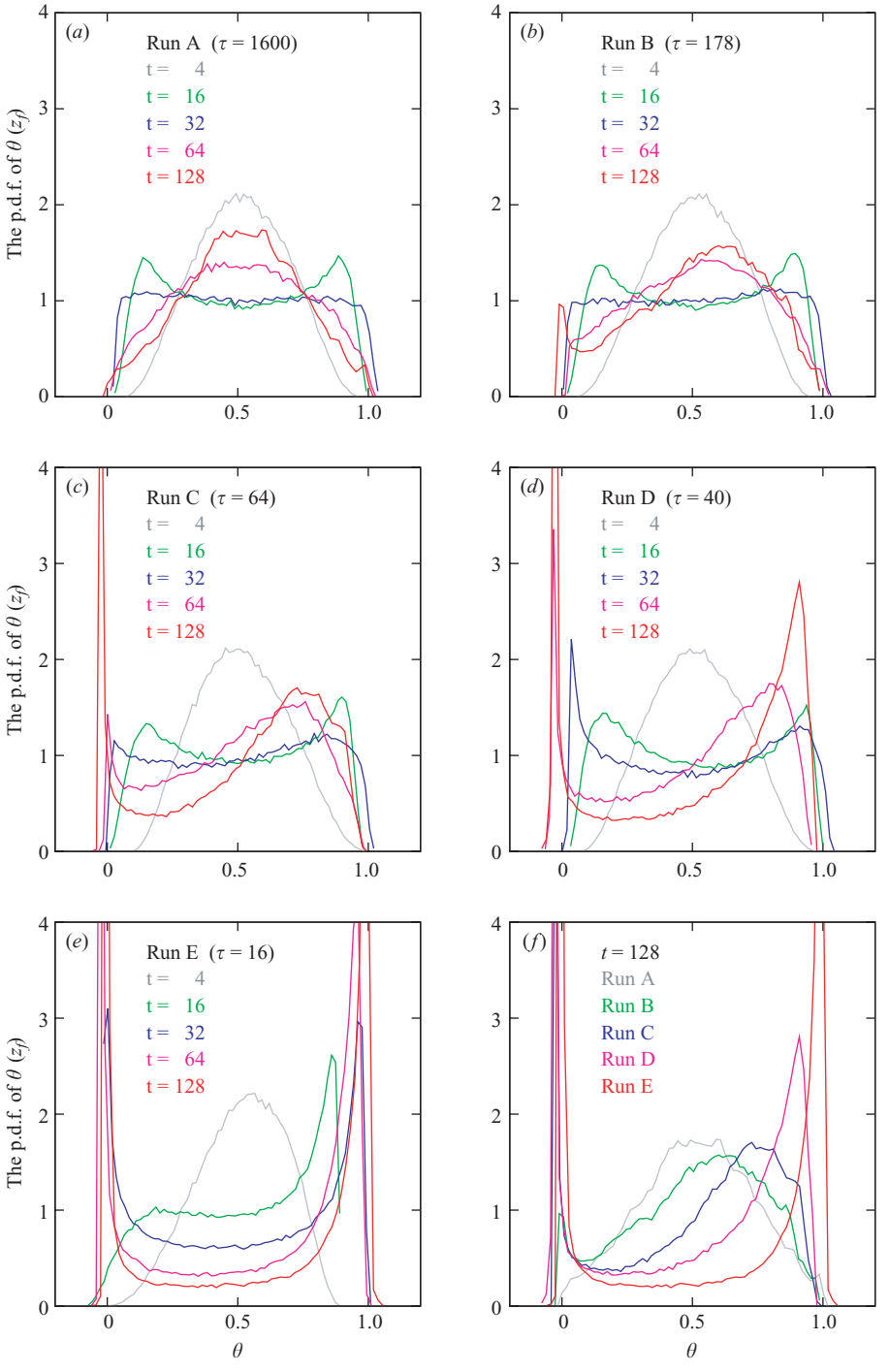


FIGURE 5. The p.d.f. of temperature in the middle slice. (*a*)–(*e*) Time evolution of the p.d.f.s. (*f*) Comparison of the p.d.f.s at $t = 128$ for different reaction times τ.

https://doi.org/10.1017/S0022112009007666 Published online by Cambridge University Press

temperature fields and temperature p.d.f.s to direct measurements of reaction efficiency and turbulent flame thickness.

4. Phenomenology

This section focuses on analysis of the asymptotic ($t \gg \tau$), segregated regime, supposedly characterized by extended inertial interval and scaling behaviours. The simulations discussed above do not run long enough to reach and accurately resolve this regime. However, the simulations are in qualitative agreement with the phenomenology constructed, thus providing a starting point for more ambitious simulations in the future.

We first review the relevant facts from 'non-reacting' RT turbulence ($\tau = \infty$). In this case the phenomenology (Chertkov 2003), supported by numerical simulations (Zingale *et al.* 2005; Cabot & Cook 2006) and some (though limited) experimental observations, can be summarized as follows. At $t \gg t_{inst}$ the width of the mixing zone grows as $H \propto t^2$. Velocity fluctuations within the mixing zone are described by the Kolmogorov cascade, whereas temperature fluctuations follow the Corrsin–Obukhov cascade. Both cascades are driven by the largest RT scale (the spikes and the bubbles) at $L_v \approx L_\theta \propto H$. Even though this driving scale grows with time, turbulence at smaller scales is adiabatically adjusted to the growth. The adiabaticity is due to the monotonic decrease of the turbulence turnover time with the scale.

As discussed above and illustrated in figure 1, for $t < \tau$ the development in the reacting case proceeds as in the benchmark non-reacting case. Here θ is well mixed within the mixing zone, and the single-point distribution of the temperature is peaked around the median value of $\theta = 1/2$. Typical fluctuations of the velocity and temperature inside the mixing zone (measured in terms of the differences $\delta_r v$ and $\delta_r \theta$ between two points separated by a distance r) are described by the Kolmogorov–Corrsin–Obukhov estimates,

$$\delta_r v \sim (L_v/t)(r/L_v)^{1/3}, \quad \delta_r \theta \sim (r/L_v)^{1/3}, \quad \text{if } L_v \gg r \gg \eta, r_d, \tag{4.1}$$

which are insensitive to the reaction. The viscous and thermal diffusion scales η and r_d can be estimated as $\eta \sim r_d \sim (\nu t)^{3/4}/L_v^{1/2} \propto t^{-1/4}$, provided the Prandtl number is of order unity.

Since the velocity correlation functions are formed by the direct cascade determined by the nonlinear term in (1.1), the driving effectively occurs at the scale $L_v \approx L_\theta$, with the former one being not very sensitive to the reaction statistics and thus determined by the same estimates as in the non-reacting case (4.1). (Weak sensitivity of the velocity statistics to the reaction was also observed in our simulations; see figure 3.) In contrast, the θ statistics are strongly modified at $t \gg \tau$ when pure-phase regions are formed separated by relatively thin interfaces (see figures 3 and 5). The interface width L_f is estimated by balancing advection and reaction terms in (1.2), $\delta_r v \delta_r \theta / r \sim \delta_r \theta / \tau$. One thus derives the following estimate for the turbulent flame thickness:

$$L_f \sim L_\theta (v_{L_\theta} \tau / L_\theta)^{3/2} \sim g \tau^{3/2} t^{1/2}. \tag{4.2}$$

The turbulent flame thickness does grow with time but in such a way that both L_θ/L_f and L_f/r_d also grow as time advances. (Although our numerical data do not run long enough to illustrate the increase of L_f with time, we did observe the increase of L_f with τ; see figure 3*f*.)

Let us now exploit the Kolmogorov–Obukhov relation, calculating the time derivative of $\theta(\boldsymbol{r}_1)\theta(\boldsymbol{r}_2)$ in accordance with (1.2) and then averaging the result over a

https://doi.org/10.1017/S0022112009007666 Published online by Cambridge University Press

slice perpendicular to the z-axis for a fixed value of $\boldsymbol{r}=\boldsymbol{r}_1-\boldsymbol{r}_2$, where $L_f \ll r \ll L$. Making use of the adiabaticity and neglecting the reactive and diffusive terms in (1.1) and (1.2) one derives

$$\nabla \langle (\boldsymbol{v}(\boldsymbol{r}_1)-\boldsymbol{v}(\boldsymbol{r}_2))(\theta(\boldsymbol{r}_1)-\langle\theta(\boldsymbol{r}_1)\rangle)(\theta(\boldsymbol{r}_2)-\langle\theta(\boldsymbol{r}_2)\rangle)\rangle \sim \varepsilon_\theta,$$

where the flux term on the right-hand side originates from driving at the large scale, $v_z\partial_z\langle\theta\rangle$, due to the large-scale temperature gradient set by buoyancy (Shraiman & Siggia 1994). Using the Kolmogorov estimation (4.1) for $\delta_r v$, one arrives at

$$S_2(r) \equiv \langle(\delta_r\theta)^2\rangle \sim \varepsilon_\theta \varepsilon_v^{-1/3} r^{2/3} \sim (r/H)^{2/3}. \tag{4.3}$$

The most important assumption, made while deriving (4.3), concerns neglecting the reactive contribution to the θ^2 balance. This assumption will be justified later in the section.

At $r \gg L_f$, (4.3) also describes the probability for two points separated by r of falling in two distinct domains of $\theta \approx 0$ and $\theta \approx 1$, or vice versa. Exactly the same probabilistic arguments apply to a temperature structure function of any positive order, thus resulting in the asymptotic independence of the respective scaling exponent of the order

$$S_n(r) \equiv \langle|\delta_r\theta|^n\rangle \sim (r/H)^{2/3}. \tag{4.4}$$

The expression implies strong intermittency of the temperature field, as the ratios $S_n/(S_2)^{n/2} \sim (H/r)^{(n-2)/3}$ all grow with scale at $n>2$. Notice that these arguments also apply to the immiscible RT, of the type discussed in Chertkov *et al.* (2005).

The expressions (4.3) and (4.4) suggest that the flame interface is fractal and, moreover, single fractal (as opposed to multi-fractal; see e.g. the discussion in Sreenivasan, Ramshankar & Meneveau 1989 and Kerstein 1991). The fractalization of the flame is properly explained by dependence of the fraction Δ_{mix} of the mixing zone on the turbulence flame thickness L_f. Taking (4.3) and (4.4) at $r \to L_f$, one estimates $\Delta_{mix} \sim (L_f/H)^{2/3} \sim \tau/t$. This also implies that $z_f \sim H$, thus confirming the general conclusion made in § 2.

Now we are ready to justify the approximation leading to (4.3). Let us estimate contribution of the flame/reaction term $\mu = \langle[\theta(\boldsymbol{r}_1)-\langle\theta(\boldsymbol{r}_1)\rangle]R(\boldsymbol{r}_2)\rangle/\tau$ to the aforementioned θ^2 balance relation. The product is non-zero only if $\boldsymbol{r}_2$ falls inside the interface. Then μ is much less than $\langle R\rangle/\tau$, since $\theta(\boldsymbol{r}_1)-\langle\theta(\boldsymbol{r}_1)\rangle$ is of order unity, and it also has zero average. The average $\langle R\rangle$ is determined by the fraction of the well-mixed region within the mixing zone, $\Delta_{mix} \sim (L_f/H)^{2/3}$. One concludes that, indeed, $\mu \ll 1/t \sim \varepsilon_\theta$ at $r \gg L_f$, thus justifying the assumption made above in deriving (4.3) and subsequently (4.4).

Turning to the discussion of the range of scales smaller than L_f but larger than r_d, one notices that the reaction term does not contribute to the θ^2 balance, as it is much smaller than the respective advection contribution. At these scales, where the direct effect of the reaction term is irrelevant and the Kolmogorov velocity estimates still survive, one expects that the Obukhov–Corrsin scaling $\delta_r\theta \propto r^{1/3}$ applies. Matching the self-similar behaviour with (4.4) at L_f, one derives the following scaling relation for the structure functions at $L_f \gg r \gg r_d$:

$$S_n(r) \sim (L_f/H)^{2/3}(r/L_f)^{n/3}. \tag{4.5}$$

This formula allows a simple interpretation: the first term on the right-hand side stands for the fraction Δ_{mix} of the well-mixed region within the mixing zone in which the reaction takes place, while the second term accounts for the Corrsin–Obukhov

https://doi.org/10.1017/S0022112009007666 Published online by Cambridge University Press

decay of correlations with the decrease in scale. The main contribution to the right-hand side of (4.5) comes from the interfacial domains, while contributions associated with pure-phase domains, where $\theta \approx 0$ or $\theta \approx 1$, are much smaller.

5. Conclusions

In this manuscript we have analysed the reactive RT turbulence in the case of a slow flame realized when the typical reaction time τ is larger then the time of RT instability development t_{inst}. The RT instability leads to formation of the mixing zone at $t \sim t_{inst}$. Further development of the mixing zone is roughly split into the early turbulent stage, $\tau \gtrsim t \gtrsim t_{inst}$, characterized by well-mixed hot and cold phases, and the later stage, $t \gtrsim \tau$, where pure state phases are segregated. In the early stage, the system is only mildly sensitive to the reaction (flame), resulting in a slight shift of the mixing zone as a whole but no visible feedback of the flame on velocity distribution. The velocity fluctuations are still insensitive to the reaction; at $t \gtrsim \tau$, however the temperature fluctuations become modified significantly. In this regime, burning takes place within thin interfaces separating large patches of pure phases. Our numerical simulations confirm the basic prediction of the transition at $t \approx \tau$. All the qualitative features expected from the transition are observed in the simulations. Given that our numerical resources were not sufficient for detailed analysis of the asymptotic, $t \gg \tau$, stage, we rely here on the phenomenology. Separation of the advective range for density fluctuations in two ranges and formation of a single-fractal flame interface are our two main phenomenological predictions. This highly intermittent behaviour of density fluctuations is in a great contrast with what was observed without reaction. These and other predictions of the phenomenology are subjects for juxtaposition with future numerical and laboratory experiments.

Notice that the general picture of mixing at $t > \tau$ discussed above is reminiscent of the immiscible turbulence discussed in Chertkov *et al.* (2005). In both cases large regions of pure phases are separated by thin interfaces. Viewed at the scales larger than the interface width, the interfaces are advected passively. Moreover, strong intermittency in the density fluctuations, reported above for the reactive case, also takes place in the setting of externally stirred (e.g. by gravity) immiscible turbulence.

Finally, our phenomenology also applies to other regimes of turbulent flames, e.g. those realized in combustion engines, where the turbulent flame width is positioned in between the integral scales of turbulence and the viscous/diffusive scales, $L_v, L_\theta \gg L_f \gg \eta, r_d$.

We wish to thank P. Fischer for the permission to use the Nekton code, A. Obabko and P. Fischer for the detailed help in using the code and V. G. Weirs for useful comments. This work was supported by the US Department of Energy at Los Alamos National Laboratory under contract no. DE-AC52-06NA25396. The work was also supported through grant no. B341495 to the Center for Astrophysical Thermonuclear Flashes at the University of Chicago and the RFBR grant 06-02-17408-a at the Landau Institute.

REFERENCES

Andrews, M. J. & Spalding, D. B. 1990 A simple experiment to investigate two-dimensional mixing by Rayleigh–Taylor instability. *Phys. Fluids* A **2**, 922–927.

Bockmann, M. & Muller, S. C. 2004 Coarsening in the buoyancy-driven instability of a reaction-diffusion front. *Phys. Rev.* E **70**, 046302/1–5.

https://doi.org/10.1017/S0022112009007666 Published online by Cambridge University Press

Borghi, R. 1988 Turbulent combustion modelling. *Prog. Energy Combust. Sci.* **14**, 245–292.

Cabot, W. H. & Cook, A. W. 2006 Reynolds number effects on Rayleigh–Taylor instability with possible implications for type Ia supernovae. *Nature Phys.* **2**, 562–568.

Cetegen, B. M. & Kasper, K. D. 1996 Experiments on the oscillatory behaviour of buoyant plumes of helium and helium–air mixtures. *Phys. Fluids* **8**, 2974–2984.

Chandrasekhar, S. 1961 *Hydrodynamic and Hydrodynamic Instability*. Dover.

Chertkov, M. 2003 Phenomenology of Rayleigh–Taylor turbulence. *Phys. Rev. Lett.* **91**, 115001/1–4.

Chertkov, M., Kolokolov, I. & Lebedev, V. 2005 Effects of surface tension on immiscible Rayleigh–Taylor turbulence. *Phys. Rev.* E **71**, 055301/1–4.

Constantin, P., Kiselev, A. & Ryzhik, L. 2001 Quenching of flames by fluid advection. *Comm. Pure Appl. Math.* **54**, 1320–1342.

Constantin, P., Lewicka, M. & Ryzhik, L. 2006 Traveling waves in 2d reactive Boussinesq systems with no-slip boundary conditions. *Nonlinearity* **19**, 2605–2615.

Constantin, P., Oberman, A., Kiselev, A. & Ryzhik, L. 2000 Bulk burning rate in passive–reactive diffusion. *Arch. Rational Mech.* **154**, 53–91.

Cook, A. W. & Dimotakis, P. E. 2001 Transition stages of Rayleigh–Taylor instability between miscible fluids. *J. Fluid Mech.* **443** (2), 69–99.

Corrsin, S. 1951 On the spectrum of isotropic temperature fluctuations in an isotropic turbulence. *J. Appl. Phys.* **22**, 469–474.

Dalziel, S. B., Linden, P. F. & Youngs, D. L. 1999 Self-similarity and internal structure of turbulence induced by Rayleigh–Taylor instability. *J. Fluid Mech.* **399**, 1–48.

Damköler, G. 1940 The effect of turbulence on the flame velocity in gas mixtures. *Z. Electrochem. Angew. Phys. Chem.* **46**, 601–626.

Duff, R. E., Harlow, F. H. & Hirt, C. W. 1962 Effects of diffusion on interface instability between gases. *Phys. Fluids* **5**, 417–425.

Fisher, R. 1937 The wave of advance of advantageous genes. *Ann. Eugen.* **7**, 355–369.

Freeman, J. R., Clauser, M. J. & Thompson, S. L. 1977 Rayleigh–Taylor instabilities in inertial-confinement fusion targets. *Nucl. Fus.* **17**, 223–230.

Frisch, U. 1995 *Turbulence: The Legacy of A. N. Kolmogorov*. Cambridge University Press.

Gamezo, V. N., Khokhlov, A. M., Oran, E. S., Chtchelkanova, A. Y. & Rosenberg, R. O. 2003 Thermonuclear supernovae: simulations of the deflagration stage and their implications. *Science* **299**, 77–81.

Kerstein, A. R. 1991 Fractal dimensions of propagating interfaces in turbulence. *Phys. Rev. A* **44**, 3363–3365.

Kerstein, A. R. 2002 Turbulence in combustion processes. *Proc. Combust. Inst.* **29**, 1763–1773.

Khokhlov, A. M. 1995 Propagation of turbulent flames in supernovae. *Astrophys. J.* **449**, 695–713.

Kolmogorov, A. N. 1941 The equation of turbulent motion in an incompressible viscous fluid. *Izv. Akad. Nauk. SSSR, Ser. Fiz.* **6** (1–2), 56–58.

Kolmogorov, A. N., Petrovskii, I. G. & Piskunov, N. S. 1937 Étude del'équation de la chaleurde matière et son application à unproblème biologique. *Bull. Moskovskogo Gosudarstvennogo Univ. Mat. Mekh.* **1**, 1–25. For an English translation, see P. Pelcé (Ed.), *Dynamics of Curved Fronts*, 1988, pp. 105–130, Academic.

Lima, D., Van Saarloos, W. & De Wit, A. 2006 Rayleigh–Taylor instabilities of pulled versus pushed fronts. *Physica* D **218**, 158–166.

Linden, P. F., Redondo, J. M. & Youngs, D. L. 1994 Molecular mixing in Rayleigh–Taylor instability. *J. Fluid. Mech.* **265**, 97.

Obukhov, A. M. 1949 Structure of the temperature field in a turbulent flow. *Izv. Akad. Nauk SSSR, Geogr. Geofiz* **13**, 58–69.

Peters, N. 2000 *Turbulent Combustion*. Cambridge University Press.

Poinsot, T. & Veynante, D. 2005 *Theoretical and Numerical Combustion*. Edwards.

Ramaprabhu, P. & Andrews, M. J. 2004 Experimental investigation of Rayleigh–Taylor mixing at small Atwood numbers. *J. Fluid. Mech.* **502**, 233–271.

Ramaprabhu, P., Dimonte, G. & Andrews, M. 2005 A numerical study of the unfluence of initial perturbations on the turbulent Rayleigh–Taylor instability. *J. Fluid Mech.* **536**, 285–319.

Rayleigh, Lord 1883 Investigation of the character of the equilibrium on an incompressible heavy fluid of variable density. *Proc. Lond. Math. Soc.* **14**, 170–177.

https://doi.org/10.1017/S0022112009007666 Published online by Cambridge University Press

Ristorcelli, R. & Clark, T. T. 2004 Rayleigh–Taylor turbulence: self-similar analysis and direct numerical simulation. *J. Fluid Mech.* **507**, 213–253.

Sharp, D. H. 1984 An overview of Rayleigh–Taylor instability. *Physica D* **12**, 3–18.

Shraiman, B. & Siggia, E. 1994 Lagrangian path integrals and fluctuations in random flow. *Phys. Rev.* E **49**, 2912–2927.

Snider, D. M. & Andrews, M. J. 1996 The simulation of mixing layers driven by compound buoyancy and shear. *ASME J. Fluids Engng* **118**, 370–376.

Sreenivasan, K.R., Ramshankar, R. & Meneveau, C. 1989 Mixing, entrainment and fractal dimensions of interfaces in turbulent flows. *Proc. R. Soc. Lond.* A **421**, 79–108.

Taylor, G. 1950 The instability of liquid surfaces when accelerated in a direction perpendicular to their planes. *Proc. R. Soc. London* A **201** (1065), 192–196.

Tieszen, S. R. 2001 On the fluid mechanics of fires. *Annu. Rev. Fluid Mech.* **33**, 67–92.

Tufo, H. M. & Fischer, P. F. 2001 Fast parallel direct solvers for coarse grid problems. *J. Parallel Distrib. Comput.* **61**, 151–177.

Vladimirova, N. & Chertkov, M. 2009 Self-similarity and universality in Rayleigh–Taylor Boussinesq turbulence. *Phys. Fluids* **21**, 015102/1–9.

Vladimirova, N., Constantin, P., Kiselev, A., Ruchayskiy, O. & Ryzhik, L. 2003 Flame enhancement and quenching in fluid flows. *Combust. Theory Modelling* **7**, 487–508.

Vladimirova, N. & Rosner, R. 2005 Model flames in the Boussinesq limit: the case of pulsating fronts. *Phys. Rev.* E **71**, 067303/1–4.

Williams, F. A. 1985 *Combustion Theory*. Benjamin Cummings.

Wilson, P. N. & Andrews, M. J. 2002 Spectral measurements of Rayleigh–Taylor mixing at small Atwood number. *Phys. Fluids* **14**, 938–945.

Young, Y. N., Tufo, H., Dubey, A. & Rosner, R. 2001 On the miscible Rayleigh–Taylor instability: two and three dimensions. *J. Fluid Mech.* **447**, 377–408.

Zingale, M., Woosley, S. E., Rendleman, C. A., Day, M. S. & Bell, J. B. 2005 Three-dimensional numerical simulations of Rayleigh–Taylor unstable flames in type Ia supernovae. *Astrophys. J.* **632**, 1021–1034.

https://doi.org/10.1017/S0022112009007666 Published online by Cambridge University Press